Sensors and Actuators B 155 (2011) 606–611

Contents lists available at ScienceDirect

Sensors and Actuators B: Chemical

journal homepage: www.elsevier.com/locate/snb

Synthesis of novel $SnO_2/ZnSnO_3$ core–shell microspheres and their gas sensing properities

Peng Sun [a], Yanfeng Sun [a], Jian Ma [a], Lu You [a], Geyu Lu [a,*], Wuyou Fu [b], Minghui Li [b], Haibin Yang [b,**]

[a] College of Electronic Science and Engineering, Jilin University, Changchun 130012, People's Republic of China
[b] State Key Laboratory of Superhard Materials, Jilin University, Changchun 130012, People's Republic of China

ARTICLE INFO

Article history:
Received 18 November 2010
Received in revised form 2 January 2011
Accepted 9 January 2011
Available online 19 January 2011

Keywords:
$SnO_2/ZnSnO_3$
Nanostructure
Hydrothermal method
Gas sensor

ABSTRACT

Large-scale novel core–shell structural $SnO_2/ZnSnO_3$ microspheres were successfully synthesized by a simple hydrothermal method with the help of the surfactant poly(vinyl pyrrolidone) PVP. The as-synthesized samples were characterized using X-ray powder diffraction (XRD), scanning electron microscopy (SEM), transmission electron microscopy (TEM), and high-resolution transmission electron microscopy (HRTEM). The results indicate that the shell was formed by single crystalline $ZnSnO_3$ nanorods and the core was formed by aggregated SnO_2 nanoparticles. The effects of PVP and hydrothermal time on the morphology of $SnO_2/ZnSnO_3$ were investigated. A possible formation mechanism of these hierarchical structures was discussed. Moreover, the sensor performance of the prepared core–shell $SnO_2/ZnSnO_3$ nanostructures to ethanol was studied. The results indicate that the as-synthesized samples exhibited high response and quick response-recovery to ethanol.

1. Introduction

Direct synthesis of nano- or microsized material with controlled shape and morphology has attracted considerable interest, because it is well-known that the properties of material depend not only on their composition, but also on their structure, phase, shape, and size [1–4]. For example, isotropic or anisotropic behavior and region-dependent surface reactivity are strongly related to the size, shape, and dimensionality of materials. Functional materials with novel morphology can be used to exploit new potential applications. To fabricate the complex architectures based on one-dimensional nanostructures or hierarchical, various strategies have been employed successfully to assemble building blocks into different morphology. However, these approaches usually involve costly templates or raw materials and complex operating steps, which possibly result in the increased cost and further limit the potential applications. Therefore, the development of a novel, facile, and low cost route to synthesis nanostructure materials, control of their shapes, and exploration underlying growth mechanisms are very important issues for understanding relationships between the materials morphologies/structures and their properties and smart assembling of nanomaterials toward their effective applications.

Tin oxide (SnO_2) and zinc stannate ($ZnSnO_3$), as famous multifunctional materials, have recently attracted considerable attention due to interesting technological properties and potential applications in various fields [5]. It is well-known that the size and morphology of such materials very strongly affect their properties and applications [3,6]. Recently, several methods have been employed to prepare SnO_2 and $ZnSnO_3$ nano- and microstructures, including template-directed, vapor–liquid–solid (VLS), chemical–vapor-deposition (CVD), thermal evaporation, and solution-phase chemical methods. Of these techniques, hydrothermal method is one of the most promising routes, due to its low cost and potential advantage for large-scale production. It is believed that gas sensing properties of nanomaterials can be enhanced by modulating the morphology [7]. On the other hand, synthesis nanomaterial with controlled shape is a facile and effective way to improve the sensitivity toward the target gas. Tin and zinc compound oxides with special nanostructures show high sensing performance to the detected gas due to the ultrahigh surface to volume ratio. Thus, it has been extensively reported for synthesis the mixture of the two oxides with various morphologies [8,9]. However, little attention has been given to the synthesis of core–shell structural $SnO_2/ZnSnO_3$ microspheres and exploration of their sensing properties.

In this paper, we report a large-scale preparation of $SnO_2/ZnSnO_3$ composite nanostructures using $SnCl_2$ as a precursor via a poly(vinyl pyrrolidone) (PVP)-assisted hydrothermal method. In the preparation process, only water, which was friendly to human health and the environments, was used as the solvent. The

* Corresponding author. Tel.: +86 431 85167808; fax: +86 431 85167808.
** Corresponding author. Tel.: +86 431 85168763; fax: +86 431 85168258.
E-mail addresses: lugy@jlu.edu.cn (G. Lu), yanghb@jlu.edu.cn (H. Yang).

0925-4005/$ – see front matter © 2011 Elsevier B.V. All rights reserved.
doi:10.1016/j.snb.2011.01.017

as-prepared products are illuminated in terms of their crystallinity, morphology, and structure. Moreover, the formation process has been investigated through the morphology evolution with different reaction times, and a possible formation mechanism is proposed. Excellent ethanol sensing properties of sensors based on these SnO_2/$ZnSnO_3$ nanostructures have been observed.

2. Experimental

2.1. Synthesis and characterization of SnO_2–$ZnSnO_3$

$Zn(CH_3COO)_2{\cdot}2H_2O$, $SnCl_2{\cdot}2H_2O$, NaOH, poly(vinyl pyrrolidone) (PVP M_W = 30,000) and hydrogen peroxide (H_2O_2 30 wt.% in H_2O) (Beijing Chemical Reagent Company) were used as received without further purification. In a typical process, PVP (1.2 g), H_2O_2 (5 mL), $Zn(CH_3COO)_2{\cdot}2H_2O$ (2 mmol), and $SnCl_2{\cdot}2H_2O$ (6 mmol) were added into 40 mL of an NaOH aqueous solution (containing 1.44 g NaOH). The solution was transferred into a Teflon-lined stainless-steel autoclave and maintained at at 180 °C for 12 h. After the hydrothermal procedure, the autoclave cooled naturally down to room temperature. The white precipitates were collected by centrifugation and washed for several times with absolute ethanol and distilled water, respectively. Subsequently, the products were dried in air at 80 °C for 12 h for further characterization.

X-ray power diffraction (XRD) analysis was conducted on a Rigaku D/max-2500 X-ray diffractometer with Cu Kα radiation (λ = 1.5418 Å). Field emission scanning electron microscopy (FESEM) images were recorded on a JEOL JSM-7500F microscope operating at 15 kV. The energy dispersive X-ray spectrometry (EDX) result was measured by the FESEM attachment. Transmission electron microscopy (TEM), selected-area electron diffractive (SAED), and high-resolution transmission electron microscopy (HRTEM) images were obtained on a JEOL JEM-200EX microscope with accelerating voltage of 200 kV and a JEOL JEM-3010 microscope operated at 200 kV, respectively. The nitrogen adsorption–desorption isotherm and Barrett–Joyner–Halenda (BJH) method were analyzed on a Micromeritics Gemini VII apparatus (Surface Area and Porosity System).

2.2. Fabrication and measurement of sensor

A gas sensor was fabricated as follows: the as-synthesized sample was mixed with water and then coated on a ceramic tube on which two platinum wires had been installed at each end. To keep the sensor working at elevated temperature, a Ni–Cr alloy coil was inserted into the ceramic tube as a heater. The gas-sensing properties of the sensor were measured with a RQ-2 gas-sensing characterization system. The measurement was processed with a static method: the sensor was put into a closed glass chamber and a given amount of the tested gas was injected into the chamber for the measurement of the sensitive performance. The gas response S is defined as the ratio R_a/R_g, where R_a and R_g are the resistances measured in air and the tested gas atmosphere. The response and recovery time are defined as the time taken by the sensor to achieve 90% of the total resistance change in the case of adsorption and desorption, respectively.

3. Results and discussion

3.1. Structural and morphological characteristics

Fig. 1 shows a typical X-ray power diffraction (XRD) pattern of the as-prepared samples using the hydrothermal method at 180 °C for 12 h. The crystal phase of the material was the mixed oxide of SnO_2 and $ZnSnO_3$, most of the diffraction peaks could be indexed

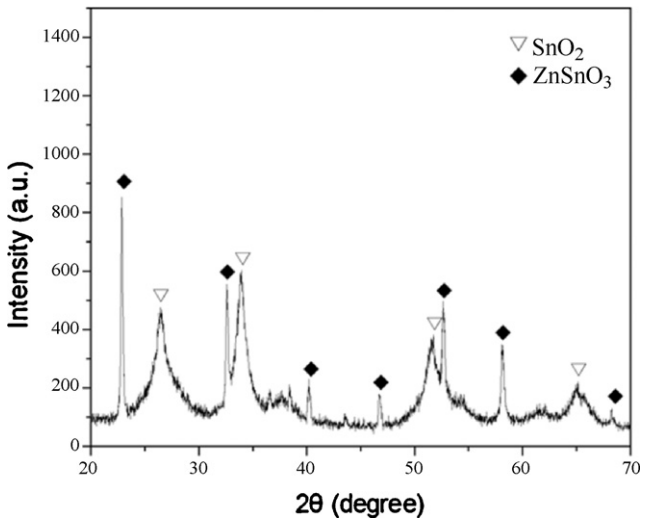

Fig. 1. XRD pattern of the as-synthesized sample.

to perovskite $ZnSnO_3$, which agreed well with the reported values from the Joint Committee on Powder Diffraction Standards card (JCPDS, 11-0274). The residual peaks were indexed to the tetragonal rutile structure of SnO_2, which was consistent with the standard date file 41-1445. Compared with those of $ZnSnO_3$, the peaks of SnO_2 were reversely broadened, which demonstrated that the SnO_2 had a small crystal size. The average crystal size was calculated to be about 7 nm using the Debye–Scherer formula, $D = 0.89\lambda/(\beta\cos\theta)$, where λ is the X-ray wavelength (1.5418 Å), θ is the Bragg diffraction angle, and β is the peak width at half maximum.

A low-magnification scanning electron microscopy (SEM) image of the as-synthesized products is shown in Fig. 2a, from which the uniform microspheres with an average diameter of 3 μm were clearly observed. No other morphologies could be detected, indicating a high yield of these microspheres. The core–shell structure could be seen more clearly from an SEM image of a broken microsphere (Fig. 2b). The complex shell was formed by nanorods with an average diameter of 50 nm, the core was formed by aggregated nanoparticles. The composition of the core was further identified by EDX measurement. The EDX result shown in Fig. 2c, it demonstrated that the peaks of O and Sn could be clearly seen in the survey spectrum. The selected-area electron diffraction (SAED) pattern of samples (Fig. 2d) shows that the as-synthesized products were polycrystalline in structure. Fig. 2e, a TEM image of a typical as-obtained nanorod, shows that it possessed sharp tip. The SAED pattern of an individual rod (inset of Fig. 2e) and high-resolution transmission electron microscopy (HRTEM) image (Fig. 2f) suggest that the nanorod was single crystalline in structure. The strong and sharp diffraction peaks in the XRD pattern and the clear lattice fringes in the HRTEM image led us to believe that the single crystalline nanorods were $ZnSnO_3$. The relatively broadened diffraction peaks in the XRD pattern, the detailed morphological characteristics in the SEM images, and the result of the EDX spectrum indicated that the aggregated nanoparticles were SnO_2.

The surface structural characteristics of the as-synthesized SnO_2/$ZnSnO_3$ core–shell structures were analyzed by nitrogen sorption isotherm techniques, Fig. 3 presents the nitrogen adsorption–desorption isotherms of the samples. As observed in Fig. 3, the core–shell structured SnO_2/$ZnSnO_3$ microspheres exhibited a type IV isotherm with a type H3 hysteresis loop for the relative pressure P/P_0 in the range 0.5–1 [10], according to the IUPAC classification, which suggested the presence of mesoporous

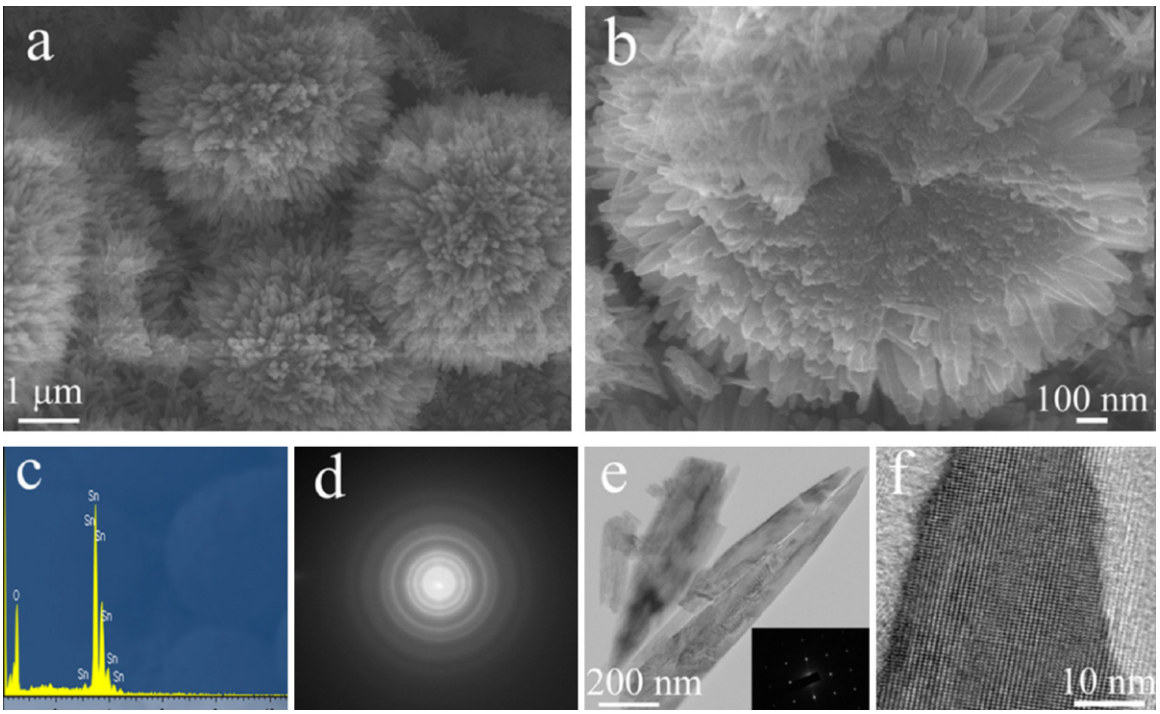

Fig. 2. (a) Low-magnification and (b) SEM image of a broken microsphere. (c) The energy dispersive spectroscopy of core. (d) The SAED pattern of samples. (e) TEM image and SAED result of nanorods. (f) HRTEM image of the nanorod.

(2–50 nm) structure in the products [11]. The inset reveals the corresponding pore size distribution. The pore size distribution curve was derived by the Barret–Joyner–Halenda (BJH) method, which revealed a correspondingly narrow pore size distribution centered at about 3.5 nm. The BET surface area of the products was calculated to be 91.6 m^2/g by the Brunauer–Emmett–Teller (BET) method.

3.2. Growth process and mechanism

To understand the formation process of $SnO_2/ZnSnO_3$ core–shell microspheres and possible growth mechanism, we investigated the evolutional morphology of the intermediates obtained after different reaction times, which is shown in Fig. 4. When the hydrothermal time was 30 min, it could be observed that the sample consisted of some irregularly polyhedron (Fig. 4a). No nanorods were observed. X-ray power diffraction (XRD) of sample (see the inset) confirmed that mainly of the diffraction peaks could be clearly indexed as $ZnSn(OH)_6$ and matched well with the reported values from the Joint Committee on Powder Diffraction Standards card (JCPDS file no. 73-2384). Weak diffraction peaks from the tetragonal SnO_2 (JCPDS file no. 41-1445) were also observed. This indicated that $ZnSn(OH)_6$ was formed at early stage. With an extension of the reaction time to 4 h, a rodlike morphology was observed and the diameter of nanorods was less than 30 nm, which was estimated from the SEM image (Fig. 4b). As the hydrothermal process was prolonged to 12 h, the hierarchical $SnO_2/ZnSnO_3$ spheres in bulk quantity were obtained (Fig. 4c), and the detailed characteristics of them are described in the above part. However, upon further increasing the reaction time to 24 h led to the formation of smooth microspheres, as shown in Fig. 4d.

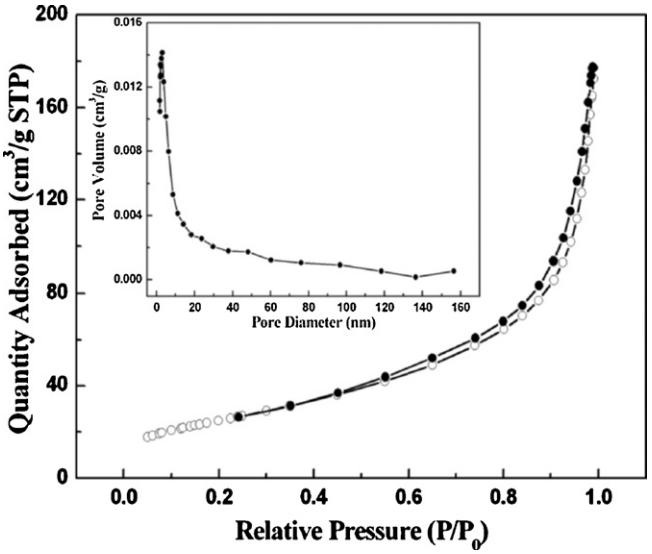

Fig. 3. Typical N_2 gas adsorption–desorption isotherm of samples. The inset is the corresponding pore-size distribution.

On the basis of the SEM and TEM observations, along with crystal structure analyses, we proposed a possible three-step growth mechanism for the formation of $SnO_2/ZnSnO_3$ core–shell spheres. The main evolving steps are schematically illustrated in Fig. 5. Firstly, $Zn(OH)_4^{2-}$ and $Sn(OH)_6^{2-}$ anions were formed by the complexation between Zn^{2+}, Sn^{4+} and OH^- ions in the strong alkaline solution. Under hydrothermal conditions, $ZnSn(OH)_6$ nuclei formed quickly, followed by the growth of the nuclei into polyhedron-shaped crystals (Fig. 5, step 1). Then, secondary nucleation occurred on the edges and surfaces of these polyhedron-shaped crystals, followed by subsequent growth of the branched structures that provided high-energy sites for nanocrystal growth (Fig. 5, step 2) [12]. Finally, the metastable $ZnSn(OH)_6$ intermediate phase decomposed and recrystallized to form different morphologies (Fig. 5, step 3) according to the "dissolution–recrystallization" mechanism [13]. The detailed mechanism for the formation of $SnO_2/ZnSnO_3$ core–shell structure is still under investigation by our group. Here is a working hypothesis that agreed with the electron microscopy.

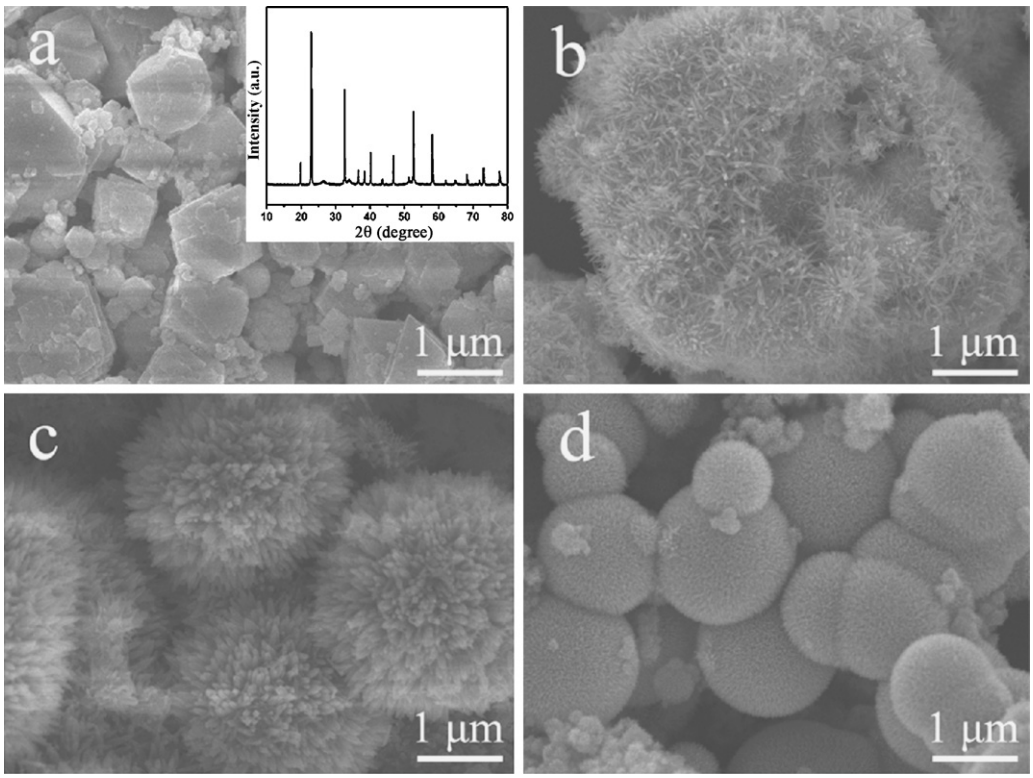

Fig. 4. SEM images of morphology evolution of samples prepared with different time: (a) 30 min, (b) 4 h, (c) 12 h and (d) 24 h. The inset of (a) shows the XRD pattern of the as-synthesized sample at 30 min.

To understand the effect of PVP on the formation of well-defined hierarchical structures, the controlled experiments had been carried out. The results indicate that the amount of PVP was crucial in the synthesis, while keeping other experimental conditions unchanged. By adjusting the amount of PVP, samples with different morphologies could be obtained accordingly. When no PVP was used, it could be observed that the samples consisted of some agglomerates (Fig. A.1a, supplementary materials). Even when the hydrothermal time was prolonged, the morphology of products was still preserved. As 0.4 g PVP was introduced into the reaction system, it can be seen that these agglomerates transformed into the rodlike shapes with the diameter of about 20–30 nm, although a small amount of products remained the aggregated nanoparticles (Fig. A.1b, supplementary materials). Further increased in the amount of PVP (0.8 g and 1.2 g) led to the generation of relatively regular spheres, which were constructed by many one-dimensional nanorods with an average diameter of 50 nm (Fig. A.1c–d, supplementary materials), and nearly no aggregated nanoparticles could be observed. Therefore, on the basis of the morphological study, it can be concluded that PVP plays an important role in forming SnO_2/$ZnSnO_3$ core–shell structure.

3.3. Ethanol sensing properties

The schematic drawing of the sensor tested is shown in (Fig. A2, supplementary materials), and the details of fabrication are described in the experimental section. The gas sensing properties of SnO_2/$ZnSnO_3$ core–shell structure were investigated. Fig. 6 shows the gas response of the sensor based on SnO_2/$ZnSnO_3$ core–shell structure to volatile organic compound (VOC) testing gases, such as ethanol, acetone, methanol, etc. All of the gases were tested at an operating temperature of 275 °C with a concentration of 100 ppm. In Fig. 6, the results indicate that the sensor exhibited little responses to acetone and formaldehyde, and were almost insensitive to methanol, butanone, xylene, and chloroform. The highest response of the sensor was 36.5 to ethanol, while the responses to other gases were no greater than 12. From the results, it is concluded that the selectivity of the sensor to ethanol against other VOC gases was exceeding almost by 3 times.

It is well known that the response of a semiconductor gas sensor is greatly influenced by operating temperature. At low temperatures the tested gas molecules are not activated enough to overcome the activation energy barrier to react with the adsorbed

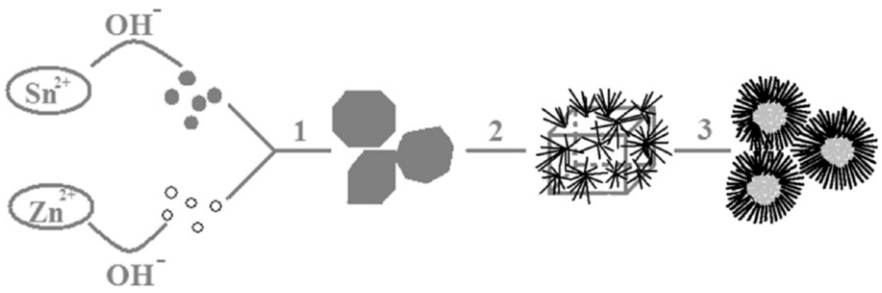

Fig. 5. Schematic illustration of the formation process of hierarchical SnO_2–$ZnSnO_3$ nanostructures.

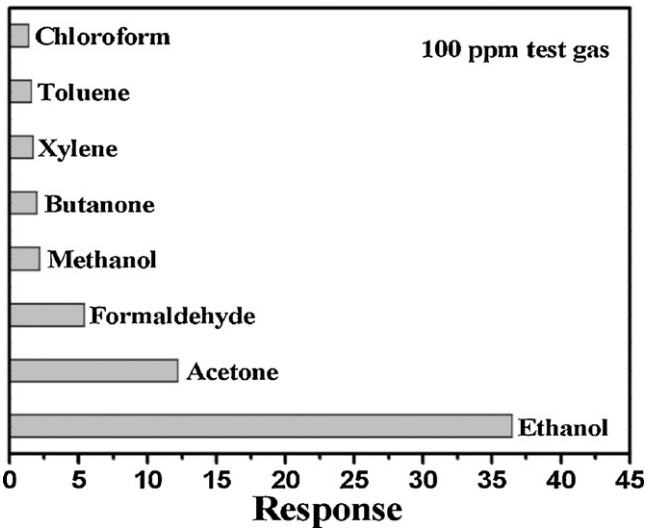

Fig. 6. Response of the sensor to different test gases.

oxygen species, while at temperatures which are too high the difficulty in gas adsorption is not adequately compensated by the increased surface reactivity [14–17]. In order to determine the optimum operating temperature, the response of the $SnO_2/ZnSnO_3$ core–shell structure gas sensor to 100 ppm ethanol vapor was tested as a function of operating temperature, as shown in Fig. 7a. It is obvious that the response to ethanol increased with the operating temperature, which attained the maximum at 275 °C, and then decreased with a further rise of the operating temperature. Therefore, a temperature of 275 °C was believed to be the optimum operating temperature for the detection of ethanol, which was applied in all the investigations hereinafter. Response of the gas sensors depends on the concentration of the tested gas, too. In this study, therefore, different gas concentrations were tested at the optimum temperature. The results are shown in Fig. 7b. It is obvious that the sensor had a wide detection range for ethanol from 20 to 1000 ppm. When the concentration of ethanol was in the range of 20–90 ppm, the responses showed good linearity with the increasing concentration (the inset of Fig. 7b). With increasing concentration of ethanol, the responses greatly increased. However, the responses slowly tended to saturation when concentrations reached higher levels.

Response and recovery times are also important parameters of a gas sensor, Fig. 8a shows the response transients of sensor to 20 ppm ethanol at 275 °C, and the results indicate that the $SnO_2/ZnSnO_3$ sensor had a fast response-recovery process. The response and recovery time of the sensor based on the as-fabricated $SnO_2/ZnSnO_3$ hierarchical structures were about within 3 and 30 s, respectively. The three reversible cycles of the response curve indicated a stable and repeatable characteristic, as shown in the inset

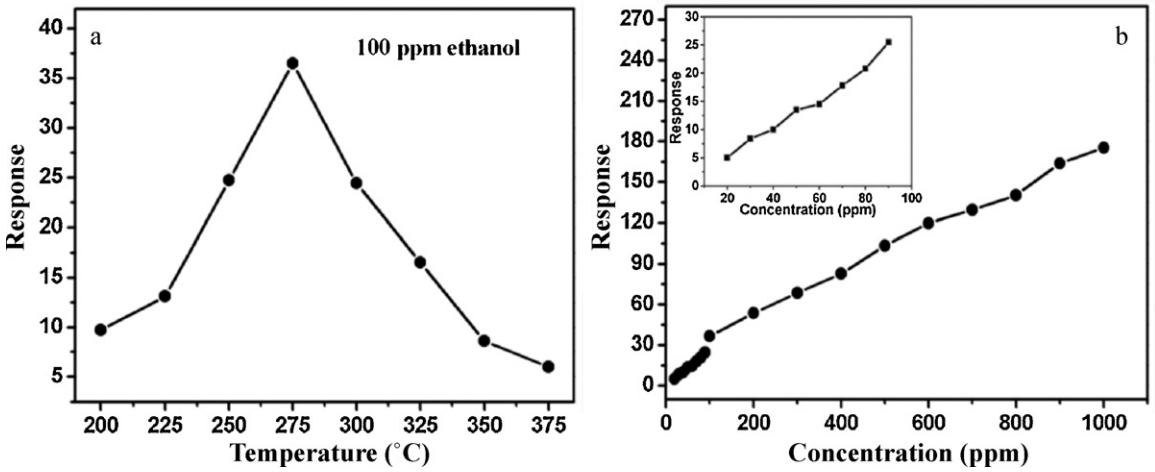

Fig. 7. (a) Response versus operating temperature of the sensor exposing to 100 ppm ethanol. (b) Relationship between response of sensor and ethanol concentration.

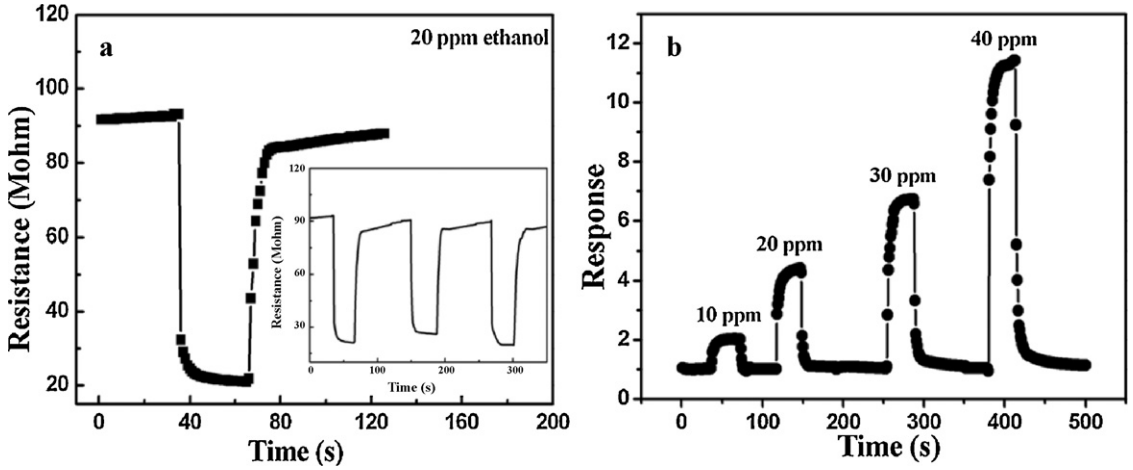

Fig. 8. (a) Response transients of the sensor to 20 ppm ethanol. The inset displaying three periods of response curve. (b) Response transients of the sensor to different concentrations of ethanol.

of Fig. 8a. The response and recovery behaviors were further investigated. Fig. 8b shows the response and recovery curves of the gas sensor upon being orderly exposed to different concentrations of ethanol at 275 °C. The responses are about 2.4, 4.8, 7.2, and 11.1 to 10, 20, 30, and 40 ppm ethanol respectively. The fast response and recovery of SnO_2/$ZnSnO_3$ sensor may be ascribed to the framework of gas diffusion toward the materials surface and its reaction with surface oxygen. The hierarchical structures provide well-defined micro- and nanoporosity for effective gas diffusion. Therefore, a fast response and recovery can be achieved using hierarchical structures.

Semiconducting metal oxides have great potential as gas-sensing materials, owing to the fact that chemical interaction of gas molecules with the semiconductor surface leads to changes in the electrical conductivity [18–21]. The unique hierarchical structures of SnO_2/$ZnSnO_3$ consisting of 1D nanorods provide efficient transport of electrons and present abundant active sites. The sensing mechanism can be considered as the following: when the SnO_2/$ZnSnO_3$ core–shell structure sensor is exposed to air, oxygen molecules can be adsorbed on its surface and capture free electrons from the conduction band to form chemisorbed oxygen species. Therefore, a space–charge region will be created on the surface of oxides, resulting in a decrease of the carrier concentration. When the sensor is exposed to a reducing gas such as ethanol at a moderate temperature, the adsorbed oxygen species on its surface will react with these gas molecules. This process releases the trapped electrons back to the conduction band and finally leads to an increase of electron concentration, which results in a decrease in the resistances.

4. Conclusions

In summary, core–shell structural SnO_2/$ZnSnO_3$ microspheres have been successfully synthesized by means of a hydrothermal method using PVP as the surfactant. The effects of PVP and hydrothermal time on the morphology of SnO_2/$ZnSnO_3$ were investigated. The results indicate that PVP plays an important role in the formation of such well-constructed microstructures. A possible formation mechanism is discussed by a three-step growth mechanism. In addition, the gas-sensing properties of our SnO_2/$ZnSnO_3$-based sensor exhibit high sensitivity, fast response, and good repeatability to ethanol.

Acknowledgements

This work was supported by the National Science Fund for Distinguished Young Scholar of China (no. 60625301) and the Jilin University Basic Research Programs of China (no. 421030991419).

Appendix A. Supplementary data

Supplementary data associated with this article can be found, in the online version, at doi:10.1016/j.snb.2011.01.017.

References

[1] W.W. Wang, Y.J. Zhu, L.X. Yang, ZnO–SnO_2 hollow spheres and hierarchical nanosheets: hydrothermal preparation, formation mechanism, and photocatalytic properties, Adv. Funct. Mater. 17 (2007) 59–64.
[2] A. Kolmskov, H.Q. Klenov, Y. Lilach, S. Stemmer, M. Moskovits, Enhanced gas sensing by individual SnO_2 nanowires and nanobelts functionalized with Pd catalyst particles, Nano Lett. 5 (2005) 667–673.
[3] Y.N. Xia, P.D. Yang, Y.G. Sun, Y.Y. Wu, B. Mayers, B. Gates, Y.D. Yin, F. Kim, H.Q. Yan, One-dimensional nanostructures: synthesis, characterization, and applications, Adv. Mater. 15 (2003) 353–389.
[4] J. Chen, L.N. Xu, W.Y. Li, X.Y. Guo, a-Fe_2O_3 nanotubes in gas sensor and lithium-ion battery applications, Adv. Mater. 17 (2005) 582–586.
[5] (a) T. Hyodo, S. Abe, Y. Shimizu, M. Egashira, Gas-sensing properties of ordered mesoporous sno$_2$ and effects of coatings thereof, Sens. Actuators B 93 (2003) 590–600;
(b) Y.L. Wang, X.C. Jiang, Y.N. Xia, A solution phase precursor route to polycrystalline SnO_2 nanowires that can be used for gas sensing under ambient conditions, J. Am. Chem. Soc. 125 (2003) 16176–16177;
(c) W.J. Moon, J.H. Yu, G.M. Choi, Selective CO gas detection of SnO_2–Zn_2SnO_4 composite gas sensor, Sens. Actuators B 80 (2001) 21–27.
[6] J.X. Huang, A.R. Tao, S. Connor, R.R. He, P.D. Yang, A general method for assembling single colloidal particle lines, Nano. Lett. 6 (2006) 524–529.
[7] X.H. Ding, D.W. Zeng, C.S. Xie, Controlled growth of SnO_2 nanorods clusters via Zn doping and its influence on gas-sensing properties, Sens. Actuators B 149 (2010) 336–344.
[8] J.Q. Xu, X.H. Jia, X.D. Lou, G.X. Xi, J.J. Han, Q.H. Gao, Selective detection of HCHO gas using mixed oxides of ZnO/$ZnSnO_3$, Sens. Actuators B 120 (2007) 694–699.
[9] Z.G. Lu, Y.G. Tang, Two-step synthesis and ethanol sensing properties of Zn_2SnO_4–SnO_2 nanocomposites, Mater. Chem. Phys. 92 (2005) 5–9.
[10] M. Kruk, M. Jaroniec, Gas adsorption characterization of ordered organic–inorganic nanocomposite materials, Chem. Mater. 13 (2001) 3169–3183.
[11] Y.G. Sun, B. Gates, B. Mayers, Y.N. Xia, Crystalline silver nanowires by soft solution processing, Nano Lett. 2 (2002) 165–168.
[12] (a) G. Xi, Y. Peng, W. Yu, Y. Qian, Synthesis, characterization, and growth mechanism of tellurium nanotubes, Cryst. Growth Des. 5 (2005) 325–328;
(b) G. Xi, K. Xiong, Q. Zhao, R. Zhang, H. Zhang, Y. Qian, Nucleation–dissolution–recrystallization: a new growth mechanism for t-selenium nanotubes, Cryst. Growth Des. 6 (2006) 577–582.
[13] Z.H. Jing, J.H. Zhan, Fabrication and gas-sensing properties of porous zno nanoplates, Adv. Mater. 20 (2008) 4547–4551.
[14] L.F. Liu, W. Wang, Q. Peng, Y.D. Li, Vanadium pentoxide nanobelts: highly selective and stable ethanol sensor materials, Adv. Mater. 17 (2005) 764–767.
[15] H. Gong, J.Q. Hu, J.H. Wang, C.H. Ong, F.R. Zhu, Nano-crystalline Cu-doped ZnO thin film gas sensor for CO, Sens. Actuators B 115 (2006) 247–251.
[16] G. Neri, A. Bonavita, G. Micali, G. Rizzo, E. Callone, G. Carturan, Resistive CO gas sensors based on In_2O_3 and InSnO*x* nanopowders synthesized via starch-aided sol–gel process for automotive applications, Sens. Actuators B 132 (2008) 224–233.
[17] N.J. Dayan, S.R. Sainkar, R.N. Karekar, R.C. Aiyer, Formulation and characterization of ZnO:Sb thick-film gas sensors, Thin Solid Films 325 (1998) 254–258.
[18] Y. Min, H.L. Tuller, S. Palzer, J. Wölenstein, H. Bötner, Gas response of reactively sputtered ZnO films on Si-based micro-array, Sens. Actuators B 93 (2003) 435–441.
[19] N. Yamazoe, New approaches for improving semiconductor gas sensors, Sens. Actuators B 5 (1991) 7–19.
[20] N. Yamazoe, G. Sakai, K. Shimanoe, Oxide semiconductor gas sensors, Catal. Surv. Asia 7 (2003) 63–75.
[21] M. Egashira, Y. Shimizu, Y. Takao, S. Sako, Variations in I–V characteristics of oxide semiconductors induced by oxidizing gases, Sens. Actuators B 35 (1996) 62–67.

Biographies

Peng Sun received his MS degree from State Key Laboratory of Superhard Materials, Jilin University, China in 2009. He entered the PhD course in 2010, majored in microelectronics and solid state electronics. Now, he is engaged in the synthesis and characterization of the semiconducting functional materials and gas sensors.

Yanfeng Sun obtained his PhD from Jilin University of China in 2007. Presently, he is working as Lecturer in Electronics Science and Engineering department of Jilin University. His current research interests are nanoscience and gas sensors.

Jian Ma received his MS in 2009 from Jilin University of China at the the Electronics Science and Engineering department. Presently, he is working as Technical Assistant in Electronics Science and Engineering department of Jilin University. His current research interests are gas sensor, the design and fabrication of micro-hot plates.

Lu You received his BS degree from the Electronics Science and Engineering department, Jilin University, China in 2010. Presently, he is a graduate student, majored in microelectronics and solid state electronics.

Geyu Lu received his BS and MS degree in electronic sciences from Jilin University, China in 1985 and 1988, respectively, and PhD degree in 1998 from Kyushu University in Japan. Now he is a full professor of Jilin University, China. Presently, he is interested in the development of functional materials and chemical sensors.

Wuyou Fu received her PhD degree from College of Chemistry at Jilin University, China in 2005. She is an associate professor in State Key Laboratory of Superhard Materials, Jilin University and interested in the field of functional nanomaterials.

Minghui Li received his BS degree from Jilin University, China in 1983. Now, he is a senior engineer in State Key Laboratory of Superhard Materials, Jilin University and interested in the field of functional nanomaterials.

Haibin Yang received his MS in materials in 1986, and PhD degree from State Key Laboratory of Superhard Materials, Jilin University, China in 1991. He is a full professor in State Key Laboratory of Superhard Materials, Jilin University and interested in the field of functional nanomaterials.